

Exposure Completing for Temporally Consistent Neural High Dynamic Range Video Rendering Supplementary Materials

Anonymous Authors

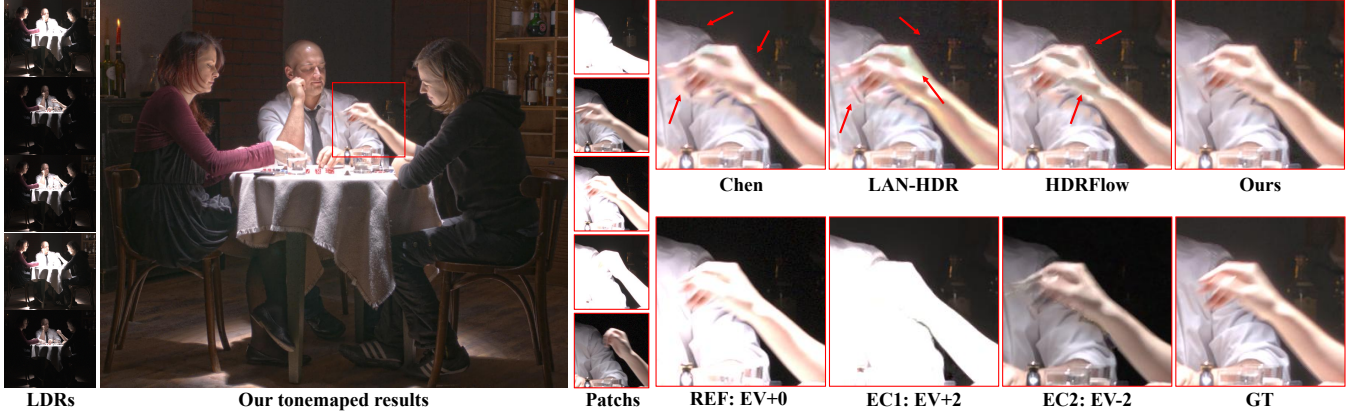


Figure 1: Qualitative comparisons of the three-exposure setting on the Cinematic Video dataset [3]. We compare our proposed method with the current state-of-the-art methods: Chen [1], LAN-HDR [2], HDRFlow [6]. REF refers to reference frame. “EV” refers to the exposure value. “EC1” and “EC2” mean the first and second completed frames with the missing exposure.

1 VIDEO RESULTS

We provide a 3-minute video comparing our HDR videos with results by other methods as an attachment in this supplementary material. One can download and play for a better view of our method.

2 NETWORK ARCHITECTURE

We provide details of the NECHDR network we proposed, mainly including the following sub-networks: feature encoder \mathcal{E} , exposure completing decoder \mathcal{D}_I , k -levels HDR rendering decoders $\{\mathcal{D}_R^k | k = 1, 2, 3, 4\}$ and blending network. Both The feature encoder \mathcal{E} and exposure-completing decoder \mathcal{D}_I are weight-shared in the two-exposure setting or the three-exposure setting. We take input LDR frames with a size of 256×256 as example and illustrate in figures for above sub-networks. In Fig. 2, 3, 4, 5, 6, 7, the parameters for “conv” and “deconv”, listed from left to right, are input channels, output channels, kernel size, stride, and padding. In our network, each “Conv” is followed by a PReLU [4], whereas there is no activation subsequent to each ‘Deconv’ layer.

In the two-exposure setting, the parameter shared feature encoder \mathcal{E} in Fig. 2 outputs pyramid features for the three input LDR frames $\{l_{t-1}, l_t, l_{t+1}\}$, while for the five input LDR frames $\{l_{t-2}, l_{t-1}, l_t, l_{t+1}, l_{t+2}\}$ in the three-exposure setting. As for the exposure completing decoder \mathcal{D}_I in the Fig. 3, we adopt the same structure and parameters in both settings. Particularly, in the three-exposure setting, the parameter shared decoder \mathcal{D}_I is utilized twice, producing two interpolated frames $\{\hat{l}_t^{e_1}, \hat{l}_t^{e_2}\}$ and theirs corresponding features $\hat{\Phi}_{t,1}^k = \{\hat{\phi}_{t,1}^k | k = 1, 2, 3\}$, $\hat{\Phi}_{t,2}^k = \{\hat{\phi}_{t,2}^k | k = 1, 2, 3\}$. The details of HDR render decoder \mathcal{D}_R^k in k levels, where $k = 1, 2, 3, 4$, are shown in Fig. 7, 6, 5, 4, respectively. In each of the Fig. 7, 6, 5, 4, the left illustrates the k -th level \mathcal{D}_R^k under two-exposure setting,

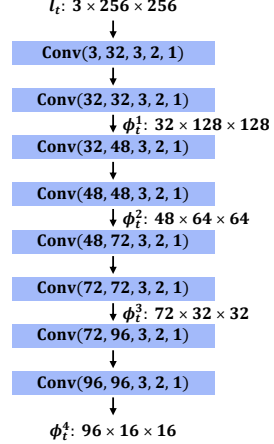


Figure 2: Details of the feature encoder \mathcal{E}

while the right is under three-exposure setting. The details regarding the blending network can be found in [6].

3 MORE QUALITATIVE COMPARISONS

Under the three-exposure setting, we provide more qualitative comparison results in Fig. 1 and Fig. 8 between our method and the current state-of-the-art approaches: Chen [1], LAN-HDR [2], HDRFlow [6]. As shown in Fig. 1, we obtain the completed frames “EC1” and “EC2”. The “EC1” provides high-exposure information with high signal-to-noise ratio to assist in removing noise from the dark background of the reference frame, while “EC2” offers low-exposure foreground object details to restore details missing due to overexposure in the reference frame. Therefore, our proposed method

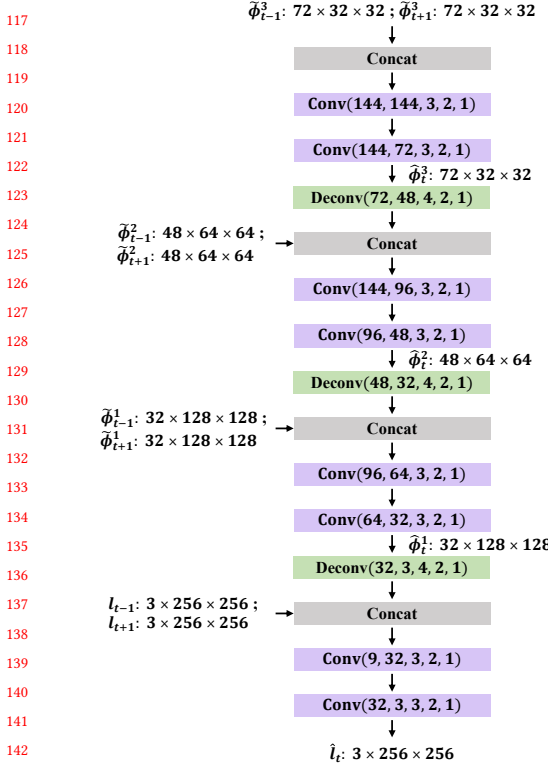
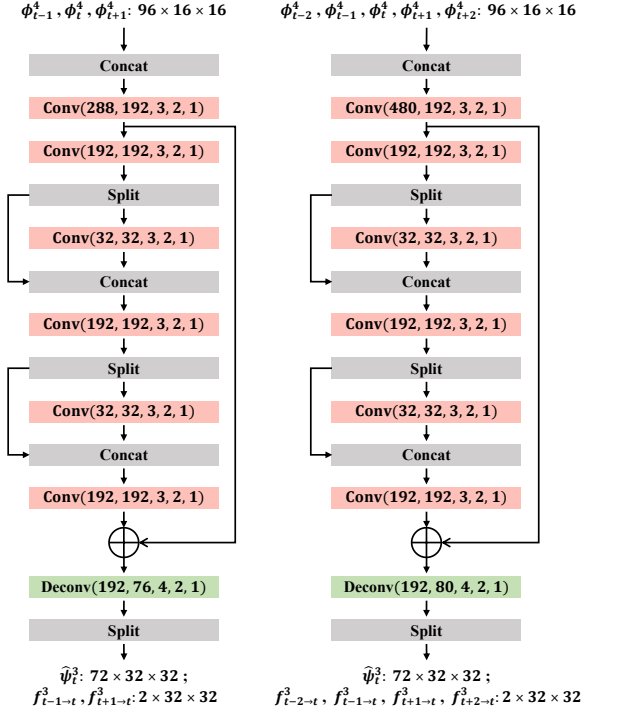
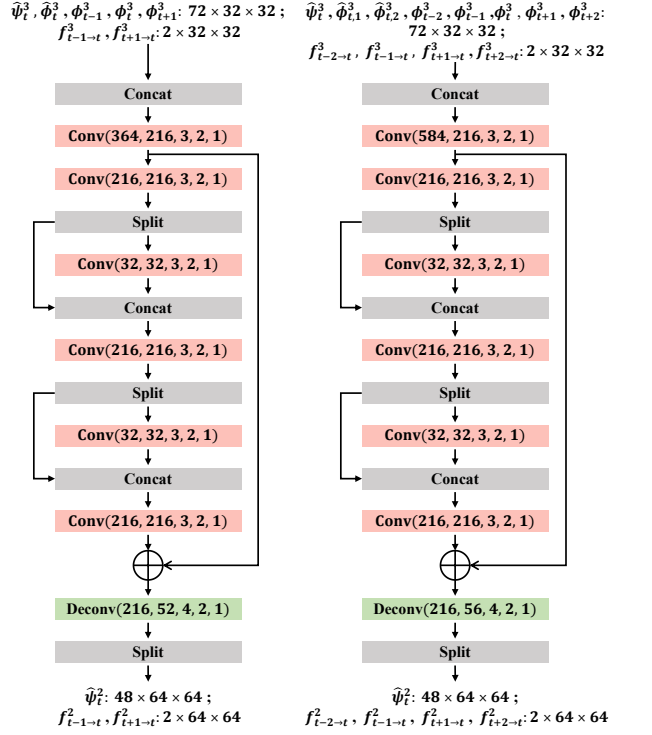
Figure 3: Details of the exposure completing decoder \mathcal{D}_I Figure 4: Details of the HDR rendering decoder \mathcal{D}_R^4 . Left: two-exposure; right: three-exposure.Figure 5: Details of the HDR rendering decoder \mathcal{D}_R^3 . Left: two-exposure; right: three-exposure.

Table 1: Quantitative comparisons on the CinematicVideo dataset [3] about parameter, inference time and performance between our “NECHDR” and the lightweight version “NECHDR-lw”.

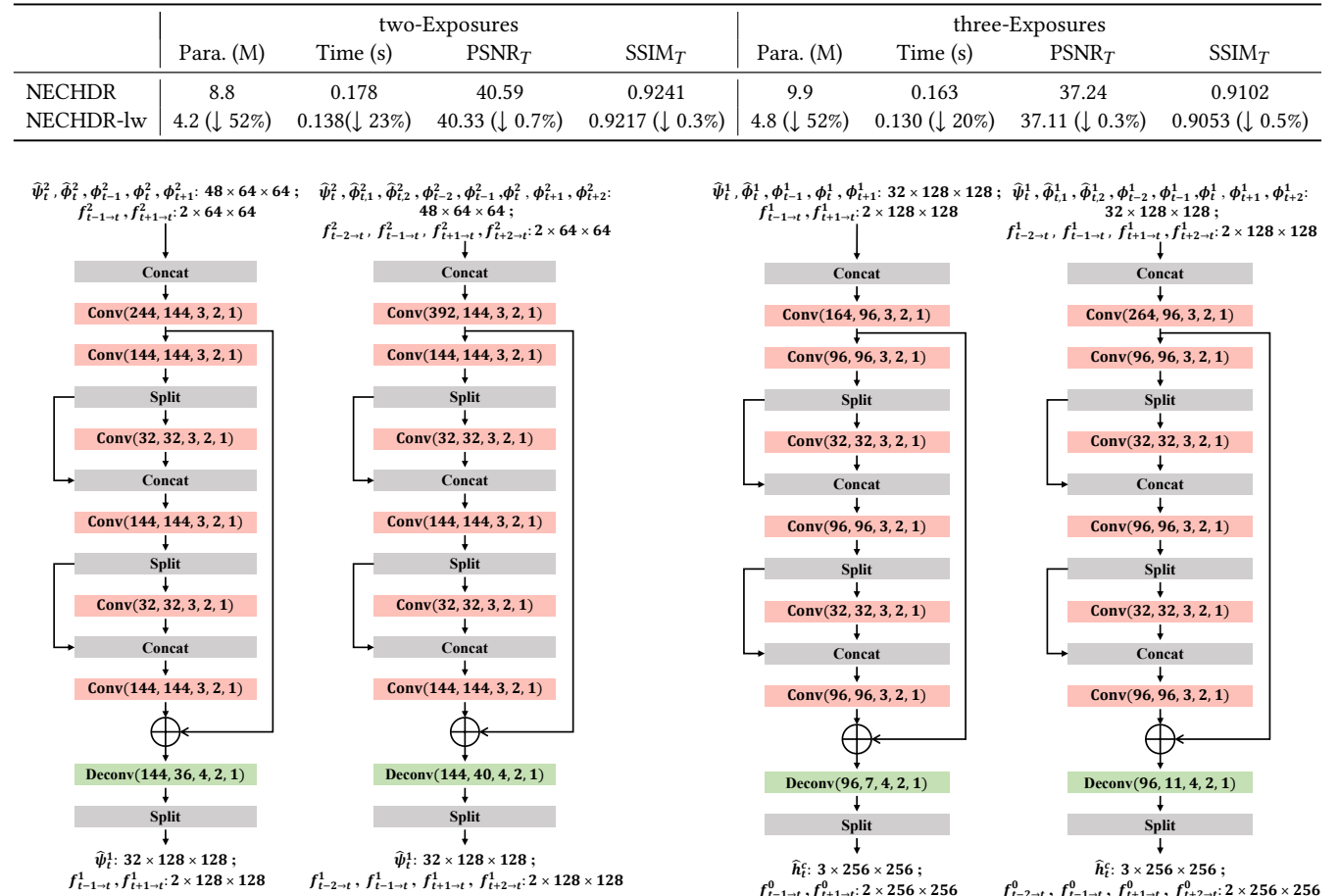


Figure 6: Details of the HDR rendering decoder \mathcal{D}_R^2 . Left: two-exposure; right: three-exposure.

Figure 7: Details of the HDR rendering decoder \mathcal{D}_R^1 . Left: two-exposure; right: three-exposure.

349 REFERENCES

- 350 [1] Guanying Chen, Chaofeng Chen, Shi Guo, Zhetong Liang, Kwan-Yee K Wong,
351 and Lei Zhang. 2021. HDR video reconstruction: A coarse-to-fine network and a
352 real-world benchmark dataset. In *Proc. Int. Conf. Comput. Vis.* 2502–2511.
353 [2] Haesoo Chung and Nam Ik Cho. 2023. LAN-HDR: Luminance-based Alignment
354 Network for High Dynamic Range Video Reconstruction. In *Proc. Int. Conf. Comput.
355 Vis.* 12760–12769.
356 [3] Jan Froehlich, Stefan Grandinetti, Bernd Eberhardt, Simon Walter, Andreas
357 Schilling, and Harald Brendel. 2014. Creating cinematic wide gamut HDR-video
358
359
360
361
362
363
364
365
366
367
368
369
370
371
372
373
374
375
376
377
378
379
380
381
382
383
384
385
386
387
388
389
390
391
392
393
394
395
396
397
398
399
400
401
402
403
404
405
406 for the evaluation of tone mapping operators and HDR-displays. In *Digital photog-*
407 *tography X*, Vol. 9023. SPIE, 279–288.
408 [4] Kaiming He, Xiangyu Zhang, Shaoqing Ren, and Jian Sun. 2015. Delving deep
409 into rectifiers: Surpassing human-level performance on imagenet classification. In
410 *Proc. Int. Conf. Comput. Vis.* 1026–1034.
411 [5] Nima Khademi Kalantari, Eli Shechtman, Connnelly Barnes, Soheil Darabi, Dan B
412 Goldman, and Pradeep Sen. 2013. Patch-based high dynamic range video. *ACM
413 Trans. Graph.* 32, 6 (2013), 202–1.
414 [6] Gangwei Xu, Yujin Wang, Jinwei Gu, Tianfan Xue, and Xin Yang. 2024. HDRFlow:
415 Real-Time HDR Video Reconstruction with Large Motions. In *Proc. IEEE Conf.
416 Comput. Vis. Pattern Recog.*
417
418
419
420
421
422
423
424
425
426
427
428
429
430
431
432
433
434
435
436
437
438
439
440
441
442
443
444
445
446
447
448
449
450
451
452
453
454
455
456
457
458
459
460
461
462
463
464



Figure 8: Qualitative comparisons of the three-exposure setting on the Cinematic Video dataset [3] and the HDRVideo dataset [5].

EC1 and EC2 mean the first and second completed frames with the missing exposure.

465
466
467
468
469
470
471
472
473
474
475
476
477
478
479
480
481
482
483
484
485
486
487
488
489
490
491
492
493
494
495
496
497
498
499
500
501
502
503
504
505
506
507
508
509
510
511
512
513
514
515
516
517
518
519
520
521
522
523
524
525
526
527
528
529
530
531
532
533
534
535
536
537
538
539
540
541
542
543
544
545
546
547
548
549
550
551
552
553
554
555
556
557
558
559
560
561
562
563
564
565
566
567
568
569
570
571
572
573
574
575
576
577
578
579
580